RESEARCH PAPER

Investigating the cell proliferation and migration inhibition by cerium oxide nanoparticles loaded with doxorubicin in MDA-MB-231 cell line

Maryam Mahdavi [1], Shahrzad Shahbazi [2], Somayeh Reiisi [1]*, Garshasb Rigi [1]

[1]Department of Genetics, Faculty of Basic Sciences, Shahrekord University, Shahrekord, Iran
[2]Division of Genetics, Department of Cell and Molecular Biology and Microbiology, Faculty of Biological Science and Technology, University of Isfahan, Isfahan, Iran

ABSTRACT

Objective(s): Cerium oxide nanoparticles (Ceo_2 NPs) are considered one of the most effective nanomaterials for drug delivery. The current study aimed to investigate the anticancer activities of doxorubicin-loaded Ceo_2 NPs (DOX-Ceo_2 NPs) against the MDA-MB-231 human breast cancer cell line.

Materials and Methods: Ceo_2 NPs were synthesized using the GREEN synthesis method and loaded with DOX (DOX-Ceo_2 NPs). The physicochemical properties of the Ceo_2 NPs were evaluated using FTIR, XRD, DLS, zeta potential, and electron microscopy (SEM/TEM). Cultured MDA-MB-231 cells were treated with different concentrations of bare Ceo_2 NPs, free DOX, and DOX-Ceo_2 NPs. In addition, HDF cells were treated with different concentrations of Ceo_2 NPs. MTT, wound healing, and flow cytometry assays were performed to determine the cell viability, migration, and apoptosis, respectively. qPCR was performed to investigate the expression of genes involved in apoptosis, including caspase (CASP) 3, 8, 9, and Bcl-2.

Results: The XRD and FTIR results confirmed the synthesis of pure and crystalline structured- Ceo_2 NPs. The average size, PDI, and zeta potential of the Ceo_2 NPs were approximately 239.1 nm, 0.074, and -9.04 mV, respectively. In vitro assays showed that DOX-Ceo_2 NPs exhibited higher cell proliferation inhibition, migration suppression, and apoptosis induction through the upregulation of CASP3, CASP8, and CASP9 genes and downregulation of Bcl-2.

Conclusion: Our data demonstrate the potential of Ceo_2 NPs for the efficient delivery of DOX and, subsequently, the improvement of its anticancer activities. Therefore, DOX-Ceo_2 NPs have the potential to be proposed as promising anticancer agents for breast cancer.

Keywords: *Breast cancer, Cerium oxide nanoparticles, Doxorubicin, Drug delivery*

INTRODUCTION

Breast cancer (BC) is one of the most common cancers and the second leading cause of cancer-related death in women worldwide [1]. There is a high degree of molecular diversity among patients with BC; that determines the risk of BC progression and resistance [2]. In many cases, chemotherapy improves the survival of BC patients. Many chemotherapeutic drugs, such as cisplatin, doxorubicin (DOX), paclitaxel, and 5-fluoracil, are used to treat BC either; individually or in combination with other drugs [3]. DOX is one of the most effective chemotherapeutic drugs currently used to treat BC, with a response rate of approximately 35% in metastatic BC [4]. However, its clinical efficacy is limited owing to adverse effects, such as cardiotoxicity, nephrotoxicity, neuropathy, hepatotoxicity, neutropenia, alopecia, and anemia [5-8]. Moreover, DOX resistance is a major problem in BC treatment and is directly associated with tumor relapse, poor prognosis, and poor survival [9, 10]. Therefore, it is necessary to develop conventional therapies along with the novel therapeutic methods. Nanotechnology is

a growing science that develops nanomaterials to improve therapeutic strategies against several diseases, such as different types of cancers, enhance the pharmacological and pharmacokinetic features of chemotherapeutic agents, and increase their efficiency without increasing their toxicity [11]. In recent decades, nanoparticles (NPs) have attracted attention because of their suitable size, shape, large surface area, and biological properties [12]. Iron-, nickel-, cerium-, and cobalt-based oxide NPs have optical and magnetic properties, and are used in several biomedical applications. These NPs can induce DNA damage and have anti-inflammatory, antioxidative, and anticancer effects [13].

Cerium oxide nanoparticles (CeO_2 NPs), known as ceria NPs, have been widely used in several fields, such as cosmetics, economy, agriculture, biology, and medicine [14-17]. Moreover, several studies have reported that CeO_2 NPs possess antioxidant [17, 18], anti-inflammatory [19, 20], antimicrobial [21, 22], antitumor [23], and drug-delivery properties [24]. They are considered promising nanocarriers for advanced drug delivery owing to their physicochemical properties, biocompatibility, and ease of production [25]. CeO_2 NPs are mostly synthesized through physical and chemical methods [26, 27]; however, these methods use toxic solvents, high temperatures, and high pressures, which are harmful to the environment, expensive procedures, low biocompatibility, and instability [22, 28]. To overcome these challenges, researchers have developed green synthesis methods using biological resources; such as plants, microbial systems, and other biological derivatives, which are safe, less toxic, and inexpensive [29].

In the current study, we synthesized CeO_2 NPs through the GREEN synthesis method and then loaded DOX into them to enhance their cytotoxicity and investigate the potential of DOX-loaded CeO_2 NPs (DOX-CeO_2 NPs) to inhibit BC cell growth, suppress migration, and induce apoptosis *in vitro*.

MATERIAL AND METHODS
Cerium oxide Nanoparticles synthesis

CeO_2 NPs were synthesized using the GREEN synthesis method. First, 0.1 M cerium nitrate hexahydrate [Ce $(NO_3)_3$ -6H$_2$O] (Sigma) was prepared with deionized water and then stirred at a medium speed. Pure Quercetin solution (10 mM) (Sigma) was prepared in ethanol 96% (Sigma) and added dropwise to cerium nitrate solution. The pH of the solution was adjusted to 10 by adding NaOH

(2M) (Merck). The obtained solution was placed on a magnetic stirrer at constant speed for 1 hr. The mixture was centrifuged at 8000 rpm for 15 min, and the precipitate was collected and washed twice with ethanol 96% and twice with distilled water. Finally, the precipitate was dried in an oven at 120 °C for an hour, and then calcined at 600 °C for 4 hr.

Nanoparticles characterization

The particle size, poly dispersive index (PDI), and zeta potential of the CeO_2 NPs were determined by dynamic light scattering (DLS) using a SZ-100 nanoparticle analyzer (Horiba, Japan). The X-ray diffraction (XRD) pattern (D8 ADVANCE X-ray diffractometer, Bruker, Germany) was used to characterize the crystalline structure of the synthesized CeO_2 NPs, analyzed at a scanning rate of 15°/min in the diffraction angle range of 10–90°. The functional groups and chemical properties of the CeO_2 NPs were evaluated by Fourier transform infrared spectroscopy (FTIR) analysis in the range of 350 - 4000 cm^{-1} using a FT/IR-6300 (JASCO-Japan). Moreover, the morphology of the CeO_2 NPs was examined using scanning and transmission electron microscopy (SEM and TEM; JSM6701F, JEOL, Japan, and CM120, Netherlands).

Doxorubicin loading in nanoparticles and drug-loading efficiency

CeO_2 NPs were impregnated with DOX and designated DOX-CeO_2 NPs. To achieve this, 10 mg of DOX was combined with an equal volume of CeO_2 NPs and then stirred at medium speed for 24 hr in the dark. The final mixture was centrifuged (15000 rpm for 15 min) to eliminate the unloaded DOX. The obtained precipitate was washed several times with distilled water and maintained at -20 °C for further use. The amount of unloaded DOX solution was determined by ultraviolet (UV) absorption at 490 nm and calculated using a calibration equation. Finally, drug-loading efficiency was calculated using the following formula:

Drug release assay

The *in vitro* drug release of DOX from the CeO_2 NPs was investigated at pH=4.5 (acidic pH, as a mimic of the tumor microenvironment) and 7.2 (neutral pH, as a mimic of physiological conditions). To this end, 20 mg of DOX-CeO_2 NPs were dispersed in 500 μL of acidic/neutral Phosphate Buffer Saline (PBS; Thermo Fisher Scientific, Waltham, USA) in

a dialysis bag (with a 12 KDa cut off). The dialysis bags were then suspended in 20 mL neutral PBS and stirred in a shaking incubator at a rate of 100 rpm at 37 °C. At predetermined times (0, 0.5, 1, 2, 4, 8, 10, 12, 24, 48, and 72 hr), 1 mL of incubated buffer was withdrawn and replaced with 1 mL of fresh PBS. The amount of DOX released at each time point was determined by measuring OD at 490 nm using UV/Vis spectrophotometry. Finally, the cumulative percentage of DOX released at each time point was calculated.

Cell culture and cell cytotoxicity

MDA-MB-231 cells, known as triple-negative BC cells (ER-, PR-, HER2-) and human dermal fibroblast (HDF) as normal cells, were obtained from the Iranian Biological Resource Center (IBRC, Tehran, Iran). Both MDA-MB-231 and HDF cells were cultured in RPMI 1640 complete medium (Gibco, USA) supplemented with 10% Fetal Bovine Serum (FBS; Gibco) and 1% antibiotics (Gibco) in T25 cell culture flasks. The flasks were then incubated in a humidified incubator with 5% Co_2 to allowing cell growth.

The cytotoxic effects of CeO_2 NPs were tested in both normal (HDF) and cancer cells (MDA-MB-231), and the anti-proliferative effects of bare CeO_2 NPs, free DOX, and DOX-CeO_2 NPs on MDA-MB-231 cells were evaluated using a 3-(4,5-dimethylthiazol-2-yl)-2,5-diphenyl tetrazolium bromide (MTT) colorimetric assay. To achieve this, HDF and MDA-MB-231 cells (at a density of 8000 cells/well) were seeded into 96-well plates and incubated for 24 hr at 37 °C and 5% Co_2, allowing for cell attachment. The HDF cells were then treated with different concentrations of bare CeO_2 NPs (0, 10, 25, 50, 100, 150, 200, and 500 µg/mL) for 48 and 72 hr. MDA-MB-231 cells were then treated with various concentrations of bare CeO_2 NPs (0, 10, 25, 50, 100, 150, 200, and 500 µg/mL), free DOX (0, 0.5, 1, 2.5, 5, 10, 20, and 50 µg/mL), and DOX-CeO_2 NPs (0, 0.5, 1, 2.5, 5, 10, 20, and 50 µg/mL) for 48 hr. Twenty microliters of MTT solution (Sigma) were added to each well and incubated for 3 hr. The medium was discarded and 100µL of dimethyl sulfoxide (DMSO; Merck) was added to each well to solubilize the formazan crystals. The optical density (OD) at 490 nm was estimated using a 96-well plate reader.

Cell migration

The effects of bare CeO_2 NPs, free DOX, and DOX-CeO_2 NPs on the migration rate of MDA-MB-231 cells were determined using a wound healing assay. Briefly, MDA-MB-231 cells were seeded in 12-well plates at a density of 7×10^5 cells/well. After 24 hr, a sterile pipette tip was used to create a wound in the middle of each well. The cells were washed twice with PBS and treated with bare CeO_2 NPs, free DOX, and DOX-CeO_2 NPs at IC_{30} concentrations. Images were captured at the time intervals of 0, 24, and 48 hr after treatment. The wound closure rate was calculated using the ImageJ software.

Flow cytometry

The effects of bare CeO_2 NPs, free DOX, and DOX-CeO_2 NPs on apoptosis of MDA-MB-231 cells were determined using a Mab-Tag apoptosis kit based on Annexin V-FITC and propidium iodide (PI) dual staining. Briefly, cells were cultured in 6-well plates at 80% density and incubated for 24 hr. The cells were treated with the IC_{30} of bare CeO_2 NPs, free DOX, and DOX-CeO_2 NPs for 48 hr. The cells were trypsinized, centrifuged at 300 × g for 5 min at 37 °C, washed twice with PBS, and resuspended in 1× annexin V binding buffer. Subsequently, the cells were stained with Annexin V-FITC and PI apoptosis markers, followed by 20 min incubation in the dark, adding 400 µL of AnnexinV binding buffer, and centrifugation at 400 g for 5 min. Finally, the samples were analyzed using a flow cytometer (BD Bioscience, Ex. 488 mm and Em. 530 nm) and Flowjow 7.6.1 software.

qPCR analysis for apoptosis genes

qPCR was used to investigate the effects of bare CeO_2 NPs, free DOX, and DOX-CeO_2 NPs on the expression of apoptosis pathway genes, including caspase (CASP) genes and Bcl-2 in MDA-MB-231 cells. To this end, the cells were cultured at a density of 1×10^6 cells/well in 6-well plates and incubated for 24 hr. The cells were then treated with the IC_{30} of bare CeO_2 NPs, free DOX, and DOX-CeO_2 NPs for 48 hr, and RNA extraction was performed using RNX Plus solution. cDNA synthesis was conducted using an M-MLV reverse transcriptase kit (YTA, Tehran, Iran) and oligo- and random hexamer primers. Real-time PCR was performed using specific primers and SYBR Green Master Mix (YTA). The data were normalized to GAPDH as an internal control. Finally, the $2^{-\Delta\Delta CT}$ equation was used to measure the fold-change.

Data analysis

GraphPad Prism software (Graph Pad Software Inc., La Jolla, CA, USA) was used to analyze the statistical results and draw the graphs. Unpaired Student's t-test and one-way analysis of variance (ANOVA) were used to investigate statistical

significance, and a p-value less than 0.05 considered significant. All *in vitro* experiments were performed in triplicates.

RESULTS

Nanoparticle synthesis and characterization

CeO_2 NPs were synthesized and loaded with DOX, according to a previously described procedure. Cerium nitrate hexahydrate and quercetin were stirred for 1 hr (Fig. 1A). Centrifugation was then performed and the precipitate was washed with ethanol and distilled water. Subsequently, drying in an oven followed by

calcination at 600 °C resulted in the formation of a yellowish powder (Fig. 1B).

Fig. 2 and 3 illustrate the physicochemical properties of the synthesized NPs. The characteristic IR absorption frequencies in the spectral range of 350–4000 cm^{-1} were measured for bare CeO_2 NPs, free Dox, and DOX- CeO_2 NPs. The interaction between CeO_2 NPs and DOX after loading was also analyzed using FTIR. The FTIR spectra of DOX-CeO_2 NPs exhibited no specific peaks with those of bare CeO_2 NPs and free DOX. As shown in Fig. 2A, CeO_2 NPs showed major
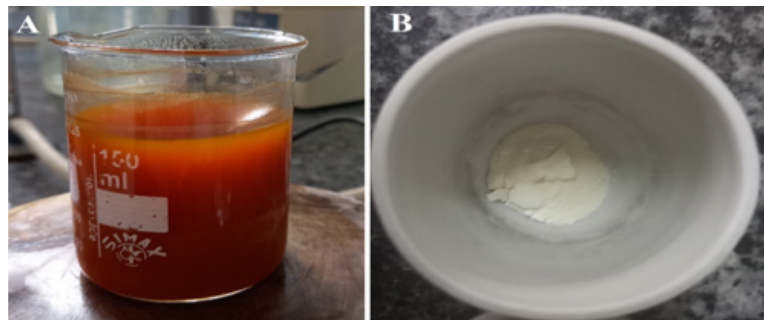

Fig. 1. CeO_2 NPs synthesis. (A) Cerium nitrate hexahydrate and prepared Quercetin were stirred for 1 hr. (B) Final white powder after drying and calcination
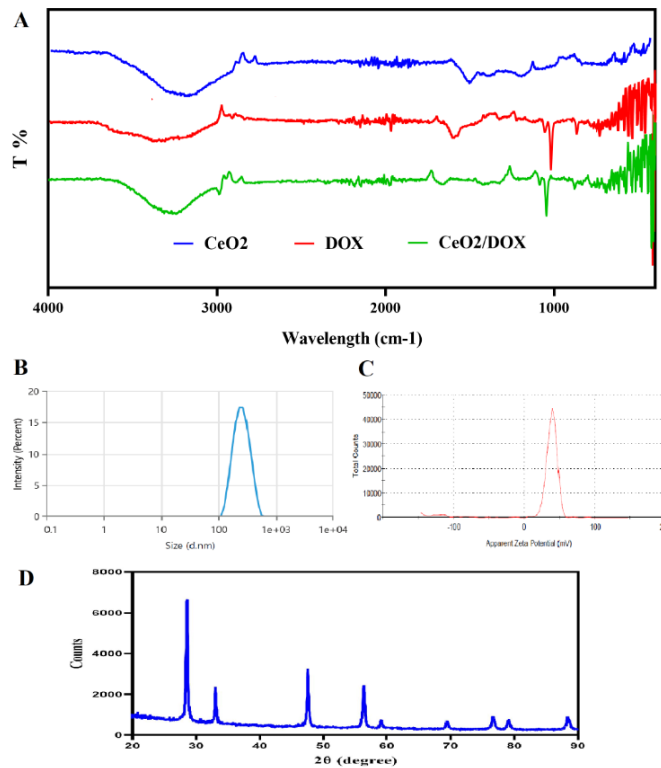

Fig. 2. Characterization of NPs. (A) FTIR spectra of bare Ceo2 NPs, free DOX, and DOX- CeO_2 NPs at a spectral range of 350-4000. (B) DLS analysis. The size and PDI of CeO_2 NPs were reported to be 239.1 nm and 0.074. (C) zeta potential of CeO_2 NPs reported to be -9.04 mV, indicating the surface charge of NPs. (D) XRD pattern of Ceo2 NPs
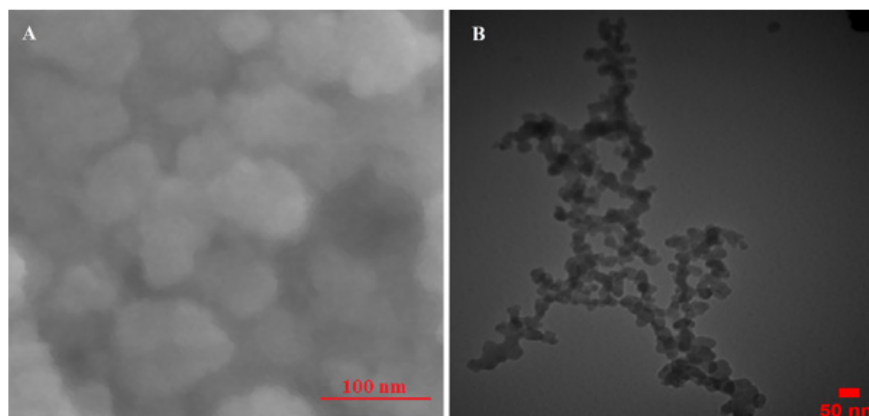
Fig. 3. Morphological analysis. (A) SEM image of Ceo2 NPs. The scale used here is 100 nm. (B) TEM image of CeO_2 NPs. The scale used here is 50 nm. These images indicate that synthesized NPs are uniform and spherical in shape

characteristic bands at 500–550 cm^{-1} owing to the Ce-O stretching vibration. Infrared absorption bands were also observed at 3433 cm^{-1} and 1627 cm^{-1} owing to the adsorption of water molecules on the nanoparticle surface. The FTIR pattern of DOX- CeO_2 NPs showed peaks corresponding to DOX. The peak at 3431 cm^{-1} could be attributed to the stretching band of the -OH groups. The peaks at 1710 cm^{-1}, 1618 cm^{-1} and 1580 cm^{-1}, and 1411 cm^{-1} are due to the stretching bands of C=O groups, bending bands of N-H groups, and C-C stretching bands, respectively. The peaks that appeared at 1284 cm^{-1}, 1208, and 984 cm^{-1} are due to the framework vibration of the carbonyl group in anthracene cycle of DOX, C-O-C asymmetric stretching vibration, and C-O stretching of the alcohol group. These results confirmed the loading of DOX onto the CeO_2 NPs. According to DLS analysis, the size of the synthesized CeO_2 NPs was reported to be 239.1 nm, which is suitable for systemic administration. Furthermore, the PDI and zeta potential of NPs were calculated to be 0.074 and -9.04 mV, respectively. The low PDI indicates that the synthesized NPs were uniform and had a homogenous size distribution, and the zeta potential demonstrated a suitable surface charge for the NPs (Fig. 2B and C).

We also performed XRD analysis to evaluate the crystalline structure of the CeO_2 NPs. Fig.2D shows the XRD pattern of CeO_2 NPs. The sharp peaks were seen at 29.08, 32.98, 47.72, 56.94, 69.84 and 77.78 respective to the (111), (200), (220), (311), (400) and (331) crystal planes. These peaks illustrate the symmetry and cubic fluorite structure of NPs. Fig.3 shows the morphology of CeO_2 NPs using SEM (Fig. 3A) and TEM (Fig. 3B) images. These results confirmed that the CeO_2 NPs were uniform and almost spherical. Boundaries

between the particles were also visible.

Drug loading and drug release

CeO_2 NPs and DOX were dispersed in a ratio 1:1, stirred for 24 hr, followed by centrifugation and extensive washing with ethanol 96% and distilled water to obtain DOX-CeO_2 NPs. The loading efficiency was calculated as 86%.

The time- and pH-dependent *in vitro* release of DOX from DOX-CeO_2 NPs was evaluated under physiological conditions (pH 7.2) and acidic conditions (pH 4.5, as a mimic of the tumor microenvironment) using dialysis bags. The concentration of DOX released from the CeO_2 NPs was estimated using spectroscopy. As shown in Fig. 4, there is a large difference between the release profile of DOX at pH=7.2 and pH=4.5. Under neutral conditions, there was approximately 30% release within the
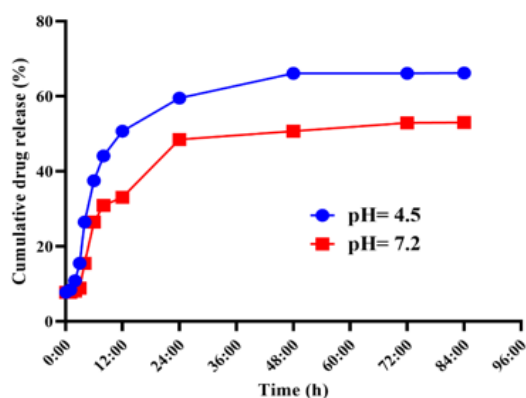

Fig. 4. *In vitro* percentage of DOX cumulative release from CeO_2 NPs. Blue and red line indicates pH=4.5 and pH=7.2, respectively. In neutral conditions there was approximately 30% release within the first 12 hr, with it reaching 45% after 24 hr, and peaking at approximately 50% at 72 hr. In acidic condition, about 65% within 72 hr

first 12 hr, reaching 45% after 24 hr; and peaking at approximately 50% at 72 hr. This is in contrast to the release profile of DOX-CeO$_2$ NPs at pH= 4.5. Under acidic conditions, the release rate of DOX from DOX-CeO$_2$ NPs became much faster, and the cumulative release of DOX from DOX-CeO$_2$ NPs reached as high as about 65% within 72 hr, which was approximately 1.5 times higher than that observed at pH 7.4. The results indicated that DOX was released slowly, that was because of a strong interaction between the drug and NPs. It has also been demonstrated that the release of DOX from DOX-CeO$_2$ NPs is pH-sensitive. The experiment was concluded after 84 hr; because no more DOX was released after this time.

Cell proliferation inhibition

The *in vitro* cytotoxicity of bare CeO$_2$ NPs against HDF cells and the antitumor activity of bare CeO$_2$ NPs, free DOX, and DOX-CeO$_2$ NPs against MDA-MB-231 cells were investigated using the MTT assay. As shown in Fig. 5a, the viability of HDF treated with CeO$_2$ NPs was approximately 90-100% at all tested concentrations from 0 to 500μg/mL after 48 and 72 hr of treatment, indicating no significant cytotoxic effect on normal cells. Fig.5B shows the anticancer effects of bare CeO$_2$ NPs on MDA-MB-231 cancer cells. Cells were treated with

0-500 μg/mL bare CeO$_2$ NPs for 48 and 72 hr. Bare CeO$_2$ NPs decreased the viability of MDA-MB-231 cells in a concentration- and time-dependent manner. The IC$_{50}$ (concentration required for 50% cell death) of bare CeO$_2$ NPs after 72 hr of treatment was calculated to be 257.60 μg/mL. Fig. 5C compares the effects of free DOX and DOX-CeO$_2$ NPs on MDA-MB-231 cells viability. The cells were then treated with various concentrations of free DOX and DOX-CeO$_2$ NPs for 48 hr. The results indicated that both free DOX and DOX-CeO$_2$ NPs inhibited the survival of MDA-MB-231 cells in a concentration-dependent manner; and that DOX-CeO$_2$ NPs were more potent than free DOX. The IC$_{50}$ values of free DOX and DOX-CeO$_2$ NPs were calculated to be 3.33 and 2.25 μg/mL, respectively, confirming the higher anticancer potential of DOX-CeO$_2$ NPs in decreasing the viability of MDA-MB-231 cells compared to free DOX.

Cell migration retardation

The effects of bare CeO$_2$ NPs, free DOX, and DOX-CeO$_2$ NPs on the migration rate of MDA-MB-231 cells were evaluated using a wound healing assay. MDA-MB-231 cells in the scratched wells were treated with the IC$_{30}$ of bare CeO$_2$ NPs, free DOX, and DOX-CeO$_2$ NPs. Fig. 6A shows the wound closure rate and cell migration observed
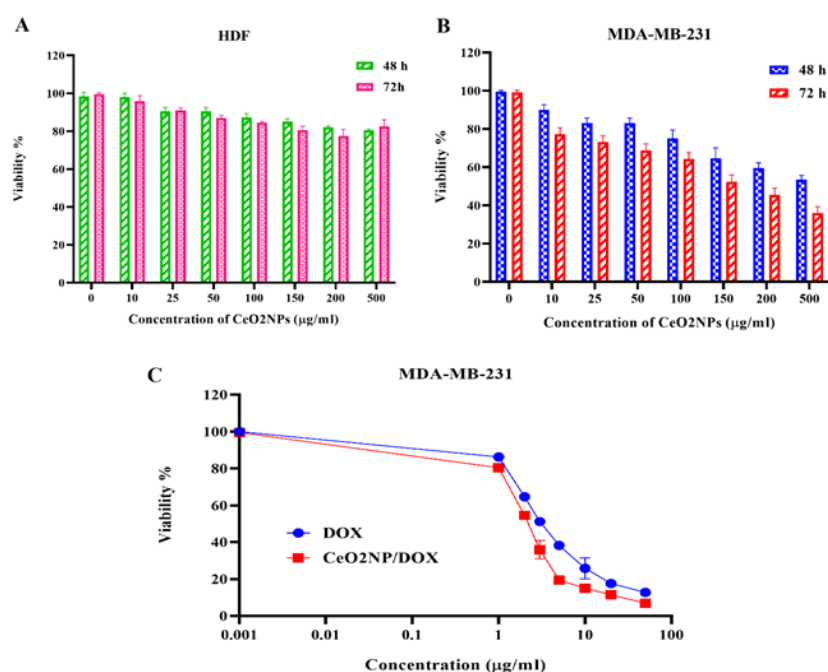

Fig. 5. (A) *in vitro* cytotoxicity of CeO$_2$ NPs (at 0-500 μg/mL concentrations) on HDF cells after 48 and 72 hr. (B) anti-proliferative effect of CeO$_2$ NPs (at 0-500 μg/mL concentrations) on MDA-MB-231 cells, after 48 and 72 hr of treatment. (C) anti-proliferative effect of free DOX and DOX-CeO$_2$ NPs on MDA-MB-231 cells, after 48 hr of treatment
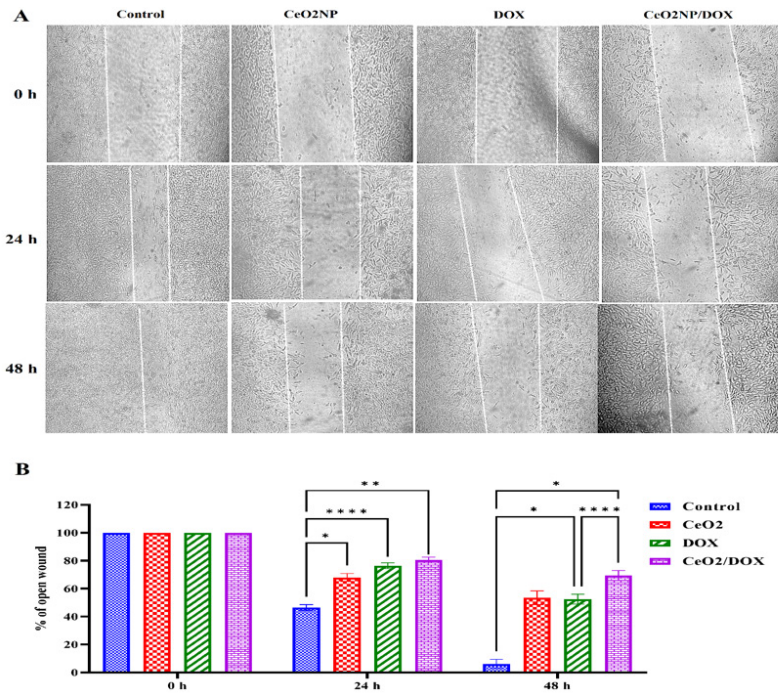
Fig. 6. Migration determination. (A) Cell morphology and migration rate after 0, 24, and 48 hr of treatment with bare CeO$_2$ NPs, free DOX, and DOX- CeO$_2$ NPs under a light microscope. (B) Wound healing scratch width ratio after 0, 24, and 48 hr treatment of bare CeO$_2$ NPs, free DOX, and DOX- CeO$_2$ NPs were analyzed using image J software. *, **, and **** revealed P-value < 0.05, 0.001, and <0.0001respectively

under a light microscope after 0, 24, and 48 hr of treatment. The scratch width ratio was calculated using ImageJ software using the mean of three individual experiments (Fig. 6B). Based on these results, bare CeO$_2$ NPs and free DOX significantly inhibited the migration of MDA-MB-231 cells after 24 and 48 hr compared to that in the control group. Furthermore, DOX-CeO$_2$ NPs were more effective in inhibiting migration than bare CeO$_2$ NPs and free

DOX (P<0.0001) because of their larger scratched area.

Cell apoptosis induction

The differences in bare CeO$_2$ NPs-, free DOX-, and DOX-CeO$_2$ NPs-induced cell deaths were determined by Annexin V-FITC/PI double staining analysis at a test concentration of IC$_{30}$. As shown in Fig. 7, bare CeO$_2$ NPs and free DOX resulted in
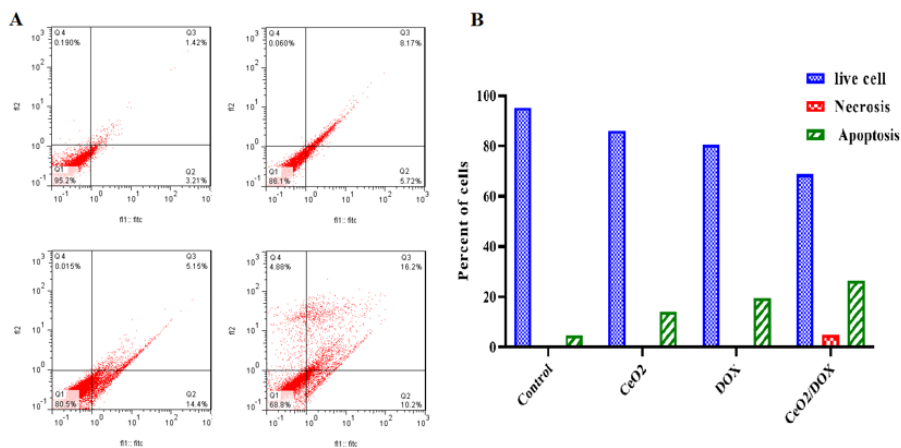

Fig. 7. (A) Effect of bare Ceo$_2$ NPs, free DOX, and DOX-CeO$_2$ NPs treatment on apoptosis induction in MDA-MB-231 cells. Quadrants (Q): Q1, live cells/Q$_2$, early apoptotic cells/Q3, late apoptotic cells/Q4, necrotic cells. (B) The total percentage of apoptotic cells after treatment with bare CeO$_2$ NPs, free DOX, and DOX-CeO$_2$ NPs
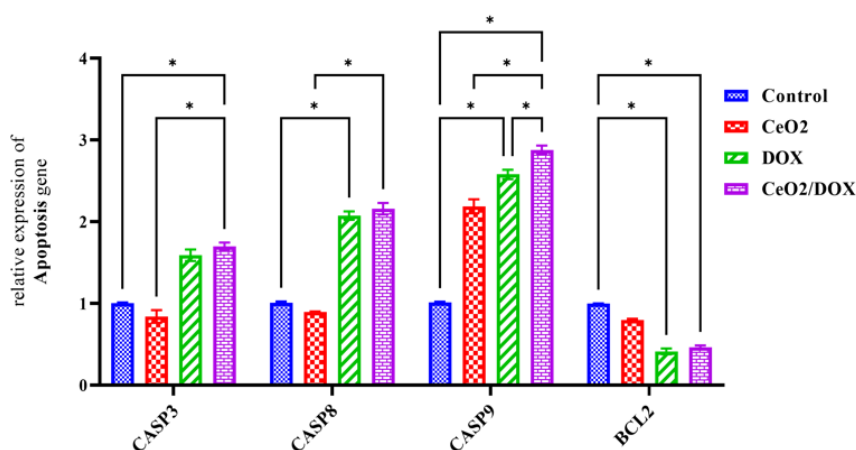
Fig. 8. CASP3, CASP8, and CASP9 and bcl-2 expression assay using qPCR analysis; MDA-MB-231 cells were treated with IC_{30} concentrations of bare CeO_2 NPs, free DOX, and DOX-CeO_2 NPs for 48 hr. * indicates significant level at $P < 0.01$

13.89 and 19.55% apoptotic cells, respectively, whereas the necrotic cell population did not change and differed (~ 0%) between the control and treated groups. DOX-CeO_2 NPs treatment of MDA-MB-231 cells resulted in 26.4% apoptosis and 4.88% necrosis, confirming the higher potential of DOX-CeO_2 NPs to induce apoptosis compared to bare CeO_2 NPs and free DOX.

Gene expression analysis

Real-time PCR was used to investigate the effect of bare CeO_2 NPs, free DOX, and DOX-CeO_2 NPs on the expression levels of some apoptotic genes in MDA-MB-231 breast cancer cell line. As illustrated in Fig. 8, the expression of CASP genes significantly increased and BCL2 was reduced after treatment with free DOX and DOX-CeO_2 NPs (P<0.01). Regarding CASP and Bcl2 genes, the expression difference between the untreated control and bare CeO_2 NPs was not significant and no difference was observed.

DISCUSSION

Breast cancer (BC) is a common and heterogeneous neoplasm with a high mortality rate in women worldwide [1]. Doxorubicin (DOX) is one of the most effective chemotherapeutic drugs used to treat a wide array of cancers, including ovarian, breast, acute lymphoblastic leukemia, myeloblastic leukemia, lung, gastric, bladder, and bone sarcomas [30]. However, DOX resistance in cancer cells remains a key problem for effective Dox treatment [31], and several genetic and epigenetic factors are responsible for DOX resistance in cancer cells [32].

DOX also induces severe short- and long-term side effects such as cardiotoxicity, gonadotoxicity, bone marrow suppression, and gastrointestinal effects [33]. Therefore, it is necessary to identify new strategies to improve its anticancer activity, reduce drug resistance, and reduce side effects. In the last decades, nanoparticles (NPs) as a development of nanotechnology help to improve cancer treatment through early cancer diagnosis, effective delivery of chemotherapeutic drugs to cancer cells, and reduction of side effects on non-cancer cells [34, 35]. The use of inorganic or lipid NPs loaded with chemotherapeutic drugs has been extensively reported [36, 37]. Based on previous findings and the introduction of CeO_2 NPs as efficient carriers for drug delivery owing to their high stability, biocompatibility, unique surface chemistry, and beneficial application in medicine [22, 38], we aimed to study the ability of CeO_2 NPs for DOX delivery. Our experimental study started with CeO_2 NPs synthesis through a GREEN synthesis method using quercetin. The GREEN synthesis of CeO_2 NPs has been described using plant extracts, microbes, and other biological derivatives. Biological derivatives in this regard, play a crucial role in the reduction and stabilization of NPs [39, 40]. In contrast to plants and microbial methods, bio-product-based CeO_2 is much safer, scalable, and has shown excellent biocompatibility [41, 42]. However, there have been no reports on the synthesis of nanoceria using quercetin. This reductive biomolecule is a potential candidate for chelation with metals to form a gel metal precursor, and nanoscale metal oxides are synthesized after the calcination process.

To increase permeability and overcome physiological barriers, studies have indicated that NPs with 10-250 nm size are suitable for systemic administration [43]. In this study, size, PDI, and zeta potential were determined to be 239.1 nm, 0.074, and -9.04 mV, respectively, indicating the suitable size, dimension, low dispersity, and surface charge for systemic circulation. Furthermore, FTIR/XRD and SEM/TEM assays indicated the crystalline and spherical structure of the CeO_2 NPs. CeO_2 NPs were then loaded with DOX through simple electrostatic interactions. Next, the loading efficiency was calculated to be 86%, indicating the high capacity of CeO_2 NPs for loading DOX. One of the limitations of this study was the change in chemotherapy drug load under different conditions, such as drug concentration, load time, and stirrer speed, and the highest amount of load was obtained with different setups. DOX released from CeO_2 NPs was evaluated at two different pH, 4.5 and 7.2. The results indicated that DOX was released slowly, and the amount of DOX released at an acidic pH was greater than that under physiological conditions. Therefore, CeO_2 NPs showed pH-dependent drug release behavior. Cheng et al. also observed that Au NPs conjugated with DOX resulted in a faster release of DOX at acidic pH than at physiological pH [44]. Previous studies have reported that CeO_2 NPs can exhibit different surface charges at different pH values. At acidic pH, CeO_2 NPs have a positive zeta potential because of the adsorption of H^+ ions on their surfaces; however, at neutral or basal pH, the zeta potential is negative because of the adsorption of OH^- ions [45, 46]. As DOX (with a positive charge) loaded into CeO_2 NPs (with a negative surface charge) occurred at physiological pH, when DOX-CeO_2 NPs were located in an acidic environment, the interaction between DOX and CeO_2 NPs became weaker than that in the physiological environment, and hydrophilic DOX was released faster from the CeO_2 NPs surface in an acidic environment than in a physiological environment. It has also been shown that CeO_2 NPs can be switched between Ce^{4+} and Ce^{3+} based on the environment and its pH. CeO_2 NPs exhibit active switching from Ce^{4+} to Ce^{3+} when located in a low-pH environment; however, they can be switched from Ce^{3+} to Ce^{4+} or Ce^{4+} to Ce^{3+} in neutral or basal environments [47]. NPs can also act as pro- and antioxidants, depending on the acidity and neutrality of the environment, respectively. They protect normal cells from free radicals at physiological pH and exert cytotoxicity in cancer cells in acidic microenvironments. The switch reaction of Ce^{3+}/Ce^{4+} was determined to be the source of the pro- or antioxidant properties of the CeO_2 NPs [17, 18]. Giri et al. observed that the amounts of Ce^{3+} and Ce^{4+} in the formulation of CeO_2 NPs also indicated the pro- or antioxidant activity of CeO_2 NPs. They showed that CeO_2 NPs with 63% Ce^{3+} suppressed ROS generation; however, folic acid-conjugated CeO_2 NPs with 24% Ce^{3+} enhanced ROS generation, and both formulations of CeO_2 NPs resulted in a significant decrease in tumor growth and inhibition of angiogenesis in an ovarian cancer mouse model [48, 49]. Wason et al. were suggested that CeO_2 NPs act as a H_2O_2 producer in tumor microenvironment (acidic pH) and act as a H_2O_2 scavenger in normal tissues (physiological pH). CeO_2 NPs can convert superoxide free radicals to H_2O_2, but at acidic pH, their catalytic activity is suppressed, and H_2O_2 accumulates in tumor cells [50]. Therefore, it can be justified that the cytotoxic effects of DOX against cancer cells can be increased when loaded onto CeO_2 NPs. The MTT assay results indicated the antiproliferative activity of bare CeO_2 NPs, free DOX, and DOX-CeO_2 NPs against MDA-MB-231 cells in a concentration-dependent manner. Furthermore, the IC50 values of bare CeO_2 NPs, free DOX, and DOX-CeO_2 NPs were determined to be 257.60, 3.33, and 2.25, respectively, indicating that DOX loading into CeO_2 NPs increased the antiproliferative activities of both DOX and CeO_2 NPs. According to previous studies, the cytotoxicity observed at high concentrations might be due to the antioxidant properties of CeO_2 NPs that enhance the activation of the CASP3 signaling pathway, resulting in significant cancer cell death [48], because of that we used a lower concentration (IC_{30}) for further experiments to keep away of cytotoxicity of bare NPs against cancer cells. Next, a wound healing assay was performed to determine the effect of IC_{30} concentrations of bare CeO_2 NPs, free DOX, and DOX-CeO_2 NPs on the migration of MDA-MB-231 cells. Both bare CeO_2 NPs and free DOX inhibited the migration of MDA-MB-231 cells, and DOX-CeO_2 NPs exerted higher anti-migratory activity than bare CeO_2 NPs and free DOX in MDA-MB-231 cells.

Defective regulation of apoptosis is one of the main hallmarks of human cancers (42). The role of bare CeO_2 NPs and free DOX in the modulation of several apoptotic pathways has been previously

investigated [32, 51-53]. We demonstrated that bare CeO$_2$ NPs and free DOX induced 13.89% and 19.55% apoptotic cell death, respectively, and no necrosis compared to untreated cells. Moreover, DOX-CeO$_2$ NPs resulted in 26.4% and 4.88% apoptosis and necrosis, respectively. Therefore, DOX loading into CeO$_2$ NPs resulted in an increase in apoptosis and necrosis induced by both DOX and CeO$_2$ NPs. Gene expression analysis revealed upregulation of CASP3, 8, and 9 genes (involved in apoptotic pathways) and downregulation of bcl-2 after treatment with bare CeO$_2$ NPs, free DOX, and DOX-CeO$_2$ NPs. DOX-CeO$_2$ NPs were more potent than bare CeO$_2$ NPs and free DOX in increasing the expression of CASP genes and decreasing the expression of anti-apoptotic bcl-2. These results confirmed those of Das et al., who reported that DOX-CeO$_2$ NPs showed higher proliferation inhibition and apoptosis induction through the upregulation of CASP3 and CASP8 and an increase in the ratio of Bax to Bcl-2 compared to free DOX in A2780 ovarian cancer cells [54]. Our results were also consistent with those of previous studies, which indicated that loading chemotherapeutic drugs into CeO$_2$ NPs increased the anticancer activities of both bare NPs and free drugs. As reported by Saranya et al., a Cerium Oxide/Graphene Oxide hybrid demonstrated dose-dependent anticancer activity against MCF7 breast cancer cells through DNA damage and ROS generation. They also mentioned that the Cerium Oxide/Graphene Oxide Hybrid with cisplatin exerted higher cytotoxic effects, indicating effective binding of the drug and nanocomposite system [52]. *Pramanik et al.* also indicated that bare CeO$_2$ NPs resulted in MDA-MB-231 cell proliferation inhibition at only high concentration (100 μg/mL). They also reported that these NPs loaded with DOX or paclitaxel resulted in a greater decrease in cell proliferation and migration than free drugs or bare NPs [55]. *Sekeroglu et al.* also showed that CeO$_2$ NPs loaded with paclitaxel had more potential to significantly decrease proliferation, inhibit migration, and induce apoptosis in MCF7 breast cancer cells than bare CeO$_2$ NPs and free paclitaxel [56]. Foroutan et al. also reported that temozolomide-loaded CeO$_2$ NPs were more effective than free temozolomide in reducing proliferation, inducing apoptosis, arresting the cell cycle, and increasing the expression of p53 in U87 glioblastoma cells [57]. Thakur et al. observed that CeO$_2$ NPs conjugated with folic acid, functionalized with amine groups, and loaded with morin (a natural polyphenol compound) exerted higher anticancer activity against breast cancer *in vitro* and *in vivo* than bare NPs and free morin [25].

CONCLUSION

In this study, CeO$_2$ NPs synthesis was performed using quercetin, and there have been no previous reports on the synthesis of nanoceria by quercetin. In addition, to the best of our knowledge, DOX loading into CeO$_2$ NPs with this approach is novel for the drug delivery of DOX.

DOX-CeO$_2$ NPs can more effectively exert antiproliferative and antimigratory activities, induce apoptosis, and induce pro-apoptotic genes expression than free DOX. Therefore, DOX loading into CeO$_2$ NPs can be suggested for the drug delivery fields as a potential therapeutic procedure for breast cancer.

ETHICS APPROVAL

This article does not contain any studies on human or animals.

CONFLICTS OF INTEREST

The authors reported no potential conflicts of interest.

REFERENCES

1. Lukong KE. Understanding breast cancer—The long and winding road. BBA Clin. 2017;7:64-77.
2. Katchman BA. From plasma peptide to phenotype: The emerging role of quiescin sulfhydryl oxidase 1 in tumor cell biology. Arizona State University; 2012.
3. Farghadani R, Naidu R. Curcumin as an enhancer of therapeutic efficiency of chemotherapy drugs in breast cancer. Int J Mol Sci. 2022 Feb; 23(4): 2144.
4. Christowitz C, Davis T, Isaacs A, Van Niekerk G, Hattingh S, Engelbrecht A-M. Mechanisms of doxorubicin-induced drug resistance and drug resistant tumour growth in a murine breast tumour model. BMC Cancer. 2019;19(1):1-10.
5. Cai F, Luis MAF, Lin X, Wang M, Cai L, Cen C, et al. Anthracycline-induced cardiotoxicity in the chemotherapy treatment of breast cancer: Preventive strategies and treatment. Molecular and clinical oncology. 2019;11(1):15-23.
6. Renu K, Abilash V, PB TP, Arunachalam S. Molecular mechanism of doxorubicin-induced cardiomyopathy–An update. European journal of pharmacology. 2018;818:241-253.
7. Ajaykumar C. Overview on the side effects of doxorubicin. Advances in Precision Medicine Oncology. 2020.
8. Renu K, Pureti LP, Vellingiri B, Valsala Gopalakrishnan A. Toxic effects and molecular mechanism of doxorubicin on different organs–an update. Toxin Rev. 2022;41(2):650-674.

9. Gote V, Nookala AR, Bolla PK, Pal D. Drug resistance in metastatic breast cancer: tumor targeted nanomedicine to the rescue.Int J Mol Sci. 2021;22(9):4673.

10. Wang X, Zhang H, Chen X. Drug resistance and combating drug resistance in cancer. Cancer Drug Resist. 2019;2(2):141–160.

11. Wicki A, Witzigmann D, Balasubramanian V, Huwyler J. Nanomedicine in cancer therapy: Challenges, opportunities, and clinical applications. J Control Release. 2015 Feb 28:200:138-157.

12. Roco MC. Broader societal issues of nanotechnology. J Nanoparticle Res. 2003;5:181-189.

13. Mukherjee S, Liang L, Veiseh O. Recent advancements of magnetic nanomaterials in cancer therapy. Pharmaceutics. 2020;12(2):147.

14. Reed K, Cormack A, Kulkarni A, Mayton M, Sayle D, Klaessig F, et al. Exploring the properties and applications of nanoceria: is there still plenty of room at the bottom? Environmental Science: Nano. 2014;1(5):390-405.

15. Hasanzadeh L, Oskuee RK, Sadri K, Nourmohammadi E, Mohajeri M, Mardani Z, et al. Green synthesis of labeled CeO_2 nanoparticles with 99mTc and its biodistribution evaluation in mice. Life Sci. 2018;212:233-420.

16. Ma R, Zhang S, Wen T, Gu P, Li L, Zhao G, et al. A critical review on visible-light-response CeO_2-based photocatalysts with enhanced photooxidation of organic pollutants. Catalysis Today. 2019;335:20-30.

17. Nelson BC, Johnson ME, Walker ML, Riley KR, Sims CM. Antioxidant cerium oxide nanoparticles in biology and medicine. Antioxidants. 2016;5(2):15.

18. Das S, Dowding JM, Klump KE, McGinnis JF, Self W, Seal S. Cerium oxide nanoparticles: Applications and prospects in nanomedicine. Nanomedicine. 2013;8(9):1483-1508.

19. Walkey C, Das S, Seal S, Erlichman J, Heckman K, Ghibelli L, et al. Catalytic properties and biomedical applications of cerium oxide nanoparticles. Environ Sci Nano.2015;2(1):33-53.

20. Hirst SM, Karakoti AS, Tyler RD, Sriranganathan N, Seal S, Reilly CM. Anti-inflammatory properties of cerium oxide nanoparticles. Small. 2009;5(24):2848-2856.

21. Farias IAP, Santos CCLd, Sampaio FC. Antimicrobial activity of cerium oxide nanoparticles on opportunistic microorganisms: a systematic review. Biomed Res Int. 2018;2018:1923606.

22. Nadeem M, Khan R, Afridi K, Nadhman A, Ullah S, Faisal S, et al. Green synthesis of cerium oxide nanoparticles (CeO_2 NPs) and their antimicrobial applications: A review. Int J Nanomedicine. 2020:5951-5961.

23. Gao Y, Chen K, Ma J-l, Gao F. Cerium oxide nanoparticles in cancer. Onco Targets Ther. 2014; 7: 835–840.

24. Calvache-Muñoz J, Prado FA, Rodríguez-Páez JE. Cerium oxide nanoparticles: Synthesis, characterization and tentative mechanism of particle formation. Colloids and Surfaces A: Physicochemical and Engineering Aspects. 2017;529:146-159.

25. Thakur N, Sadhukhan P, Kundu M, Singh TA, Hatimuria M, Pabbathi A, et al. Folic acid-functionalized cerium oxide nanoparticles as smart nanocarrier for pH-responsive and targeted delivery of Morin in breast cancer therapy. Inorganic Chemistry Communications. 2022;145:109976.

26. Liying H, Yumin S, Lanhong J, Shikao S. Recent advances of cerium oxide nanoparticles in synthesis, luminescence and biomedical studies: a review. Journal of Rare Earths. 2015;33(8):791-799.

27. Rajeshkumar S, Naik P. Synthesis and biomedical applications of cerium oxide nanoparticles–a review. Biotechnology Reports. 2018;17:1-5.

28. Magudieshwaran R, Ishii J, Raja KCN, Terashima C, Venkatachalam R, Fujishima A, et al. Green and chemical synthesized CeO_2 nanoparticles for photocatalytic indoor air pollutant degradation. Materials Letters. 2019;239:40-44.

29. Arunachalam T, Karpagasundaram M, Rajarathinam N. Ultrasound assisted green synthesis of cerium oxide nanoparticles using Prosopis juliflora leaf extract and their structural, optical and antibacterial properties. Materials Science-Poland. 2017;35(4):791-798.

30. Sohail M, Sun Z, Li Y, Gu X, Xu H. Research progress in strategies to improve the efficacy and safety of doxorubicin for cancer chemotherapy. Expert Rev Anticancer Ther. 2021 Dec;21(12):1385-1398.

31. Yang J, Wu Y, Wang X, Xu L, Zhao X, Yang Y. Chemoresistance is associated with overexpression of HAX-1, inhibition of which resensitizes drug-resistant breast cancer cells to chemotherapy. Tumour Biol. 2017 Mar;39(3):1010428317692228.

32. Ashrafizaveh S, Ashrafizadeh M, Zarrabi A, Husmandi K, Zabolian A, Shahinozzaman M, et al. Long non-coding RNAs in the doxorubicin resistance of cancer cells. Cancer Lett. 2021;508:104-114.

33. van der Zanden SY, Qiao X, Neefjes J. New insights into the activities and toxicities of the old anticancer drug doxorubicin. FEBS J. 2021;288(21):6095-6111.

34. Devi RV, Doble M, Verma RS. Nanomaterials for early detection of cancer biomarker with special emphasis on gold nanoparticles in immunoassays/sensors. Biosensors and Bioelectronics. 2015;68:688-698.

35. Prabhu RH, Patravale VB, Joshi MD. Polymeric nanoparticles for targeted treatment in oncology: Current insights. Int J Nanomedicine. 2015:10:1001-1018.

36. Luther DC, Huang R, Jeon T, Zhang X, Lee Y-W, Nagaraj H, et al. Delivery of drugs, proteins, and nucleic acids using inorganic nanoparticles. Adv Drug Deliv Rev. 2020:156:188-213.

37. Borges A, de Freitas V, Mateus N, Fernandes I, Oliveira J. Solid lipid nanoparticles as carriers of natural phenolic compounds. Antioxidants. 2020;9(10):998.

38. Aseyd Nezhad S, Es-haghi A, Tabrizi MH. Green synthesis of cerium oxide nanoparticle using *Origanum majorana* L. leaf extract, its characterization and biological activities. Applied Organometallic Chemistry. 2020;34(2):e5314.

39. Nadeem M, Tungmunnithum D, Hano C, Abbasi BH, Hashmi SS, Ahmad W, et al. The current trends in the green syntheses of titanium oxide nanoparticles and their applications. Green chemistry letters and reviews. 2018;11(4):492-502.

40. Srikar SK, Giri DD, Pal DB, Mishra PK, Upadhyay SN. Green synthesis of silver nanoparticles: a review. Green and Sustainable Chemistry. 2016;6(01):34.

41. Kargar H, Ghasemi F, Darroudi M. Bioorganic polymer-based synthesis of cerium oxide nanoparticles and their cell viability assays. Ceramics International. 2015;41(1):1589-1594.

42. Patil SN, Paradeshi JS, Chaudhari PB, Mishra SJ, Chaudhari BL. Bio-therapeutic potential and cytotoxicity assessment of pectin-mediated synthesized nanostructured cerium oxide. Appl Biochem Biotechnol. 2016;180(4):638-654.

43. Petros RA, DeSimone JM. Strategies in the design of nanoparticles for therapeutic applications. Nature reviews Drug discovery. 2010;9(8):615-627.

44. Cheng Y, Dai Q, Morshed RA, Fan X, Wegscheid ML, Wainwright DA, et al. Blood-brain barrier permeable gold nanoparticles: an efficient delivery platform for enhanced malignant glioma therapy and imaging. Small. 2014;10(24):5137-5150.

45. Liu B, Sun Z, Huang P-JJ, Liu J. Hydrogen peroxide displacing

DNA from nanoceria: mechanism and detection of glucose in serum. J Am Chem Soc. 2015;137(3):1290-1295.

46. Zhang J, Chen G, Guay D, Chaker M, Ma D. Highly active PtAu alloy nanoparticle catalysts for the reduction of 4-nitrophenol. Nanoscale. 2014;6(4):2125-2130.

47. Karakoti A, Kuchibhatla SV, Babu KS, Seal S. Direct synthesis of nanoceria in aqueous polyhydroxyl solutions. The Journal of Physical Chemistry C. 2007;111(46):17232-17240.

48. Giri S, Karakoti A, Graham RP, Maguire JL, Reilly CM, Seal S, et al. Nanoceria: A rare-earth nanoparticle as a novel anti-angiogenic therapeutic agent in ovarian cancer. PLoS One. 2013;8(1):e54578.

49. Hijaz M, Das S, Mert I, Gupta A, Al-Wahab Z, Tebbe C, et al. Folic acid tagged nanoceria as a novel therapeutic agent in ovarian cancer. BMC Cancer. 2016;16(1):1-14.

50. Wason MS, Colon J, Das S, Seal S, Turkson J, Zhao J, et al. Sensitization of pancreatic cancer cells to radiation by cerium oxide nanoparticle-induced ROS production. Nanomedicine: Nanomedicine. 2013;9(4):558-569.

51. Alpaslan E, Yazici H, Golshan NH, Ziemer KS, Webster TJ. pH-dependent activity of dextran-coated cerium oxide nanoparticles on prohibiting osteosarcoma cell proliferation. ACS Biomaterials Science & Engineering. 2015;1(11):1096-1103.

52. Saranya J, Saminathan P, Ankireddy SR, Shaik MR, Khan M, Khan M, et al. Cerium oxide/graphene oxide hybrid: Synthesis, characterization, and evaluation of anticancer activity in a breast cancer cell line (MCF-7). Biomedicines. 2023;11(2):531.

53. Chen C, Lu L, Yan S, Yi H, Yao H, Wu D, et al. Autophagy and doxorubicin resistance in cancer. Anti-cancer drugs. 2018;29(1):1-9.

54. Das J, Choi Y-J, Han JW, Reza AMMT, Kim J-H. Nanoceria-mediated delivery of doxorubicin enhances the anti-tumour efficiency in ovarian cancer cells via apoptosis. Sci Rep. 2017;7(1):9513.

55. Pramanik N, De T, Sharma P, Alakesh A, Jagirdar SK, Rangarajan A, et al. Surface-coated cerium nanoparticles to improve chemotherapeutic delivery to tumor cells. ACS Omega. 2022;7(36):31651-31657.

56. Atlı Şekeroğlu Z, Şekeroğlu V, Aydın B, Kontaş Yedier S. Cerium oxide nanoparticles exert antitumor effects and enhance paclitaxel toxicity and activity against breast cancer cells. J Biomed Mater Res B Appl Biomater. 2023 Mar;111(3):579-589.

57. Foroutan Z, Afshari AR, Sabouri Z, Mostafapour A, Far BF, Jalili-Nik M, et al. Plant-based synthesis of cerium oxide nanoparticles as a drug delivery system in improving the anticancer effects of free temozolomide in glioblastoma (U87) cells. Ceramics International. 2022;48(20):30441-30450.